Shock Waves (2012) 22:161–172
DOI 10.1007/s00193-012-0353-3

ORIGINAL ARTICLE

Unsteady three-dimensional compressible vortex flows generated during shock wave diffraction

J. O. Reeves · B. W. Skews

Received: 21 February 2011 / Revised: 26 October 2011 / Accepted: 20 December 2011 / Published online: 29 January 2012

Abstract The results of an experimental and numerical investigation into the behaviour of the spiral vortex generated by shock wave diffraction over edges yawed to the incident shock wave are presented. Three-dimensional numerical simulations reveal significant distortion and bending of the free vortex in regions near the boundary of the flow domain, so as to meet it at a right angle. The results of numerical simulations were found to mimic the experimentally obtained photographs very well. The numerical results are used to explain the various features of the resultant flow fields, with particular emphasis placed on the behaviour and properties of the spiral vortex, as it evolves with time. The effects of bending on the structure of the vortex are examined. The rate of circulation production for the three-dimensional shock diffraction cases was calculated, and the trends observed correlated with those for the much published two-dimensional diffraction case.

Keywords Vortex · Spiral vortex · Shock diffraction

1 Introduction

The formation of a spiral vortex during the diffraction of a shock wave over a convex corner has been noted and observed for many decades, with many studies published describing the basic flow features [2,4, and many others]. However, until recently, very little work has been undertaken with specific aims of attempting to quantify the parameters evident in such vortex flows, and the majority of the work that has been published to date has been limited to two-dimensional cases. This can be attributed to a number of factors, but is primarily due to the fact that it has only become practical to obtain numerical solutions, of sufficient resolution, to the governing equations of such complex three-dimensional flows using modern, high powered computers and software. Sun and Takayama [5] showed that numerical solution of the compressible Euler equations was able to represent the vortex formed in two-dimensional shock wave diffraction very well, and from the results, vorticity and vorticity production were quantitatively calculated. Tseng and Yang [6] provided the same results for the solution of the laminar Navier–Stokes equations. Solution of the two sets of equations yielded very little difference in the results.

No published work has been found on the three-dimensional shock diffraction case, and the compressible three-dimensional vortex formed as a result.

The present study investigates the shock diffraction case in three dimensions. Experimental and numerical studies were undertaken so as to quantify the flow parameters present in shock wave diffraction over straight edges yawed to the shock propagation direction, and of curved edges of parabolic profile. The straight edges were arranged in a 'V' configuration, with the tip of the 'V' being the final point of shock diffraction. Particular attention was paid to the spiral vortex, the bending it exhibits in regions close to the wall, and the distortions caused when two vortices meet. Tests were performed for incident shock Mach numbers M_s of 1.42 and 1.65.

A discussion and description of the experiment and test cases is given in Sect. 2, and a brief discussion of theory relating to three-dimensional compressible vortices and vorticity is given in Sect. 3.

Communicated by A. Sasoh.

J. O. Reeves · B. W. Skews (✉)
Flow Research Unit, School of Mechanical, Industrial and Aeronautical Engineering, University of the Witwatersrand, PO WITS, 2050 Johannesburg, South Africa
e-mail: beric.skews@wits.ac.za

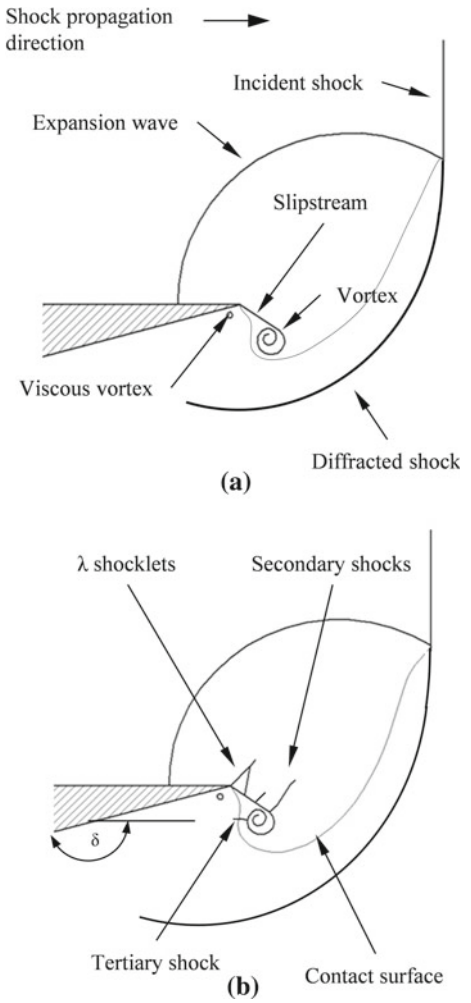

Fig. 1 Features of shock diffraction, **a** $M_s \sim 1.3$, **b** M_s from ~1.45 to 1.7

2 The experiment

The basic two-dimensional flow field for a shock wave diffracting over a convex wedge is shown in Fig. 1. This problem has become a standard test case for many numerical schemes. For incident shock Mach numbers of less than approximately 1.45, the diffraction pattern is typically that shown in Fig. 1a. For shock Mach numbers between 1.45 and 1.7, a pattern similar to that shown in Fig. 1b is evident. The two cases are similar, save for the appearance of a few additional flow features as the incident shock Mach number is increased. The λ shocklets appear for $M_s > 1.33$, becoming stronger and more visible as the incident shock strength is increased. These merge as the incident shock strength is increased further. The slipstream is formed due to the inability of the high-speed gas behind the shock wave to negotiate the corner. This forms a vortex sheet, a narrow flow region across which there is a discontinuity in tangential velocity, which extends from the tip of the diffracting edge. This rolls up to form the spiral

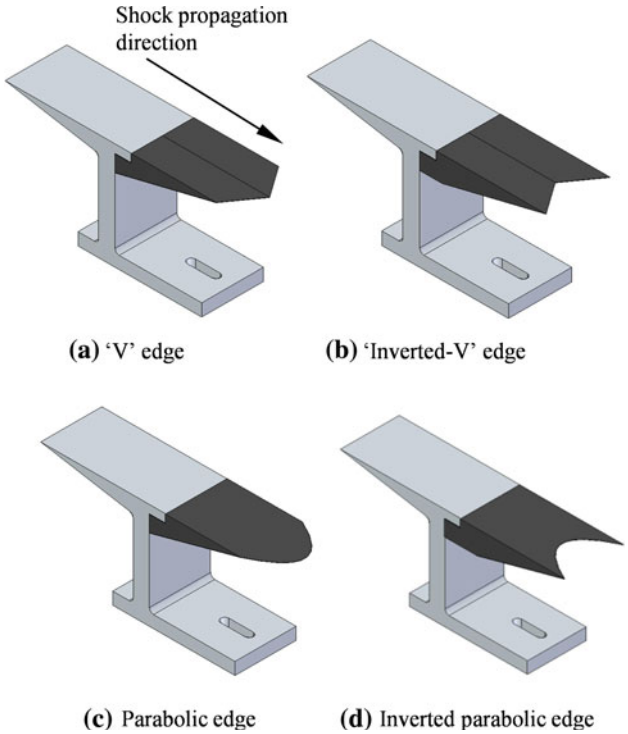

Fig. 2 Test models

vortex (labelled as vortex in Fig. 1). This feature is the primary focus of this study. For higher incident shock Mach numbers (around 1.6 and greater), secondary and tertiary shocks form in the vortex, so as to decelerate and guide the supersonic flow around the vortex.

The test models are shown in Fig. 2. The black, trailing edge portion of the model forms the wedge that the shock wave diffracts over. These models are enclosed in the test section of a shock tube, down which the incident shock wave propagates. There is thus a solid boundary on either side of the models. The wedge angle (δ, as defined in Fig. 1) was 165° for all models. Two models (Fig. 2a, b) incorporating two straight edges aligned at 45° to the incident shock, forming a 'V' and an 'inverted-V' diffracting edge were used. Two further models with edges of parabolic profile (Fig. 2c, d) were also tested. The width of the models was 76 mm, with the tip of the 'V' on the centre plane of the test section (i.e. 38 mm from either wall). The parabolic edge was defined by the relation $y = 0.0285x^2$, where x and y are in millimeters.

3 Compressible vortices

Vorticity is defined as

$$\boldsymbol{\omega} = \nabla \times \boldsymbol{u} \tag{1}$$

where $\boldsymbol{u}$ is the velocity.

A simplified form of the vorticity equation, applicable to inviscid compressible flow, is given by (2) [1].

$$\rho \frac{\mathrm{D}}{\mathrm{D}t}\left(\frac{\omega}{\rho}\right) = (\boldsymbol{\omega}\cdot\nabla)\boldsymbol{u} + \nabla T \times \nabla s \tag{2}$$

where ρ is density, T is temperature, and $\boldsymbol{s}$ is entropy.

Equation 2 describes the rate of change of vorticity for a fluid element. The first term on the right hand side states that if a vortex line is stretched, the rate of vorticity production will increase. This term is obviously zero for two-dimensional flows. The second term on the right-hand side describes an increase in vorticity if a non-zero entropy gradient is present. Whilst it is practically impossible to solve the above equation for an arbitrary flow field, it does nevertheless provide some physical explanation as to what one observes in vortex flows. It should be noted that the primary source of vorticity in the shock diffraction case is the slipstream, which is created by the singularity at the tip of the diffracting edge. This is not predicted by (2) [5].

The three laws of vortex motion were proposed by Hemholtz in 1858. An important result of the Hemholtz laws, applicable to the current study, is that the circulation around a vortex tube is constant [3]. As a result of the Stokes theorem the vorticity flux through a vortex tube is constant, or in other words, the sum of the vorticity taken on a plane perpendicular to the vortex axis inside the vortex tube is constant along the vortex axis. As such, if a vortex tube is to terminate at a solid boundary, the vortex axis would have to meet that boundary at a right angle.

This result also ties in with the first term on the right-hand side of (2), in that if a vortex tube is stretched, it will contract, and to conserve angular momentum, the rotational rate will increase. A local maximum of the vorticity vector would occur at the waist.

4 Methodology

4.1 Experimental

Experimental testing was performed in a shock tube. The test section was 180 mm tall and 76 mm wide, and had schlieren quality viewing windows of 300 mm diameter. The flow field was visualized through means of oblique schlieren photography. Schlieren images were obtained for different time instances, so as to investigate the evolution of the flow field with time. Sets of images were obtained for different viewing angles, so as to more clearly visualize the flow field, and validate the numerical results against the experimental results.

A single schlieren image was taken for each test performed, using a Fujifilm FinePix S3 Pro digital camera at a resolution of 12 megapixels. In the results that follow, sequences of images obtained for different time delays are presented. Note that each image is obtained for a separate firing of the shock tube.

Air was used as the test gas.

4.2 Numerical

The numerical results were used to explain the various features of the resultant flow fields.

Numerical simulations were performed using the commercially available Fluent 6.3.26 code. In this paper, solutions of the three-dimensional, compressible, Euler equations are shown. An explicit density-based solver, incorporating an explicit unsteady time formulation was used. A segregated solver and second-order upwind scheme were specified. An initial unstructured mesh of hexahedral cells was applied to the flow domains, with a dynamic mesh adaption scheme based on pressure gradients implemented. The adapted meshes were limited to a maximum of approximately 3.5 million hex cells, with the cell edge length in the order of 0.25 mm in the areas of maximum refinement. The dynamic grid adaptation scheme was found to track the spiral vortex and shock front satisfactorily. The computational domain corresponds to that in the experiment. Initial two-dimensional simulations were performed, so as to verify the solver settings that were to be used in the three-dimensional simulations. These two-dimensional results compared favourably with previous work by Skews [4] and Sun and Takayama [5]. Post-processing was performed in Tecplot 360.

Grid convergence was difficult to assess in these cases, due to the use of the mesh adaption scheme, the need to fine tune the mesh adaption settings during simulations, and the relatively low maximum number of cells that the computer hardware available could handle. Consistent results were obtained for models using different initial unstructured mesh densities, however, and it is felt that the results presented here represent the best that could have been achieved with the available hardware.

5 Results

The experimental and numerical results are discussed for both the parabolic and 'V' diffracting edges first. A discussion on the behaviour of the spiral vortex, and the vorticity production then follows. Discussion and data are based on the numerical results. The experimental photographs were primarily used to validate the numerical results, through comparing the schlieren images and various plots of the numerical results.

5.1 Description of flow field for parabolic models

Schlieren images for the parabolic model for $M_s = 1.65$ are given in Fig. 3. These images were obtained with an optical

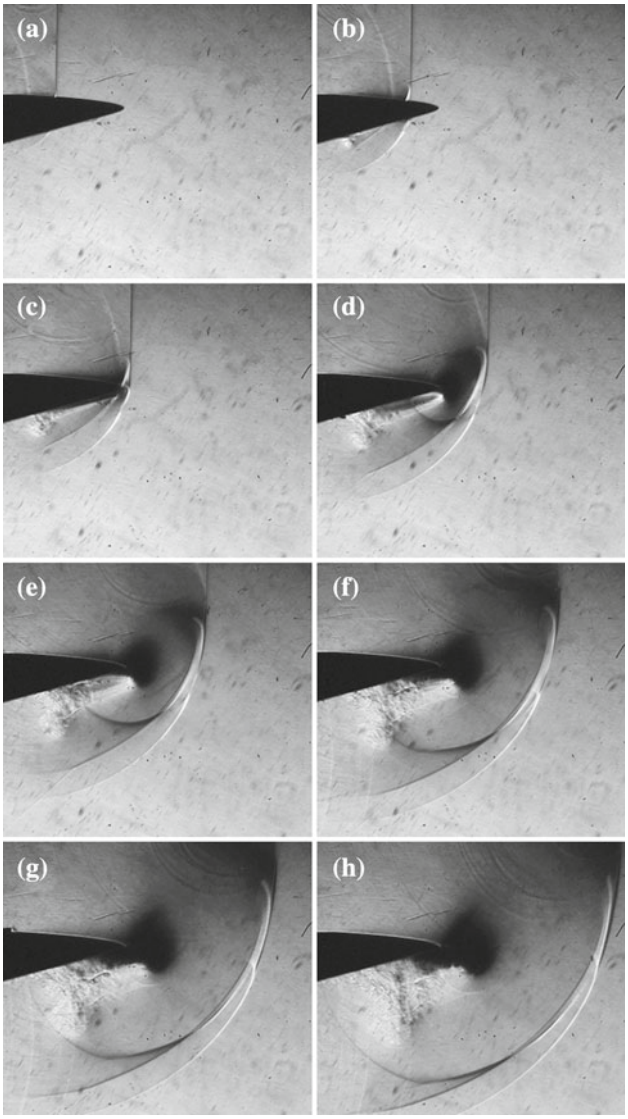

Fig. 3 Flow development, parabolic model, schlieren images taken at optical roll of 10° (optical axis rolled about the test section, so as to look down on the model at an angle of 10° to the horizontal), $\Delta t = 25\,\mu s$ between images

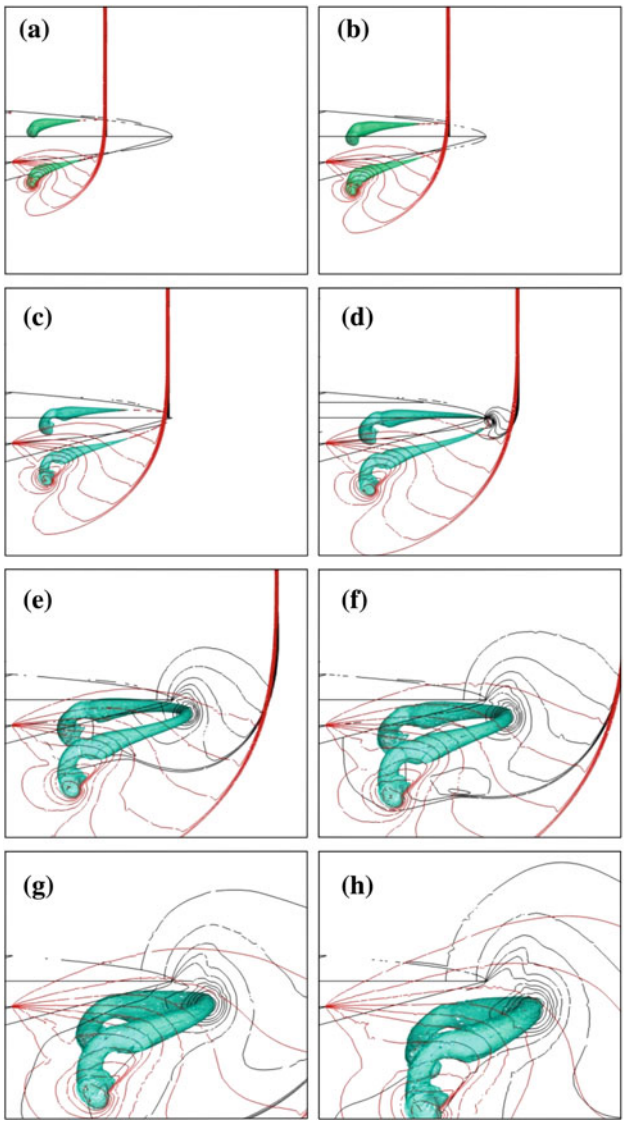

Fig. 4 Flow development, parabolic model, CFD results images, surfaces of constant density and lines of constant density (*black* centre plane, *red* near boundary) plotted ($M_s = 1.65$). Data are presented at an optical roll angle of 10°, and at the same time instants as the data in Fig. 3

roll axis inclined at 10° to the flat upper surface of the test models. The diffracted shock wave is clearly visible where it meets both the near and far windows, and on the centre plane. The behaviour of the diffracted shock wave is generally consistent with the two-dimensional diffraction case. The vortex is clearly defined in the schlieren images, and assumes a parabolic profile similar to that of the diffracting edge away from distortions caused by the presence of the windows. The vortex expands with time as it propagates downstream, and by Fig. 3h, has become less clearly defined. Secondary shocks form in the vortex in the region near the windows, so as to decelerate and guide the supersonic flow above the slipstream around the vortex. A secondary and tertiary shock form in a region near the centre plane, but are not evident anywhere else in the flow domain, aside from the region near the window. Significant distortion to the vortex is evident in a region near the windows. Here, we can see that the vortex has bent so as to meet the window, which acts as a solid boundary, at a right angle. The flow features discussed above are more clearly seen in the sequence of images generated from the numerical solution, given in Fig. 4. In the figure, the vortex is represented by the blue/green surface, and lines of constant density are shown against the near boundary in red and on the centre plane in black. The data in Fig. 4 are presented at the same optical roll angle (10°) and time instants as the schlieren images presented in Fig. 3.

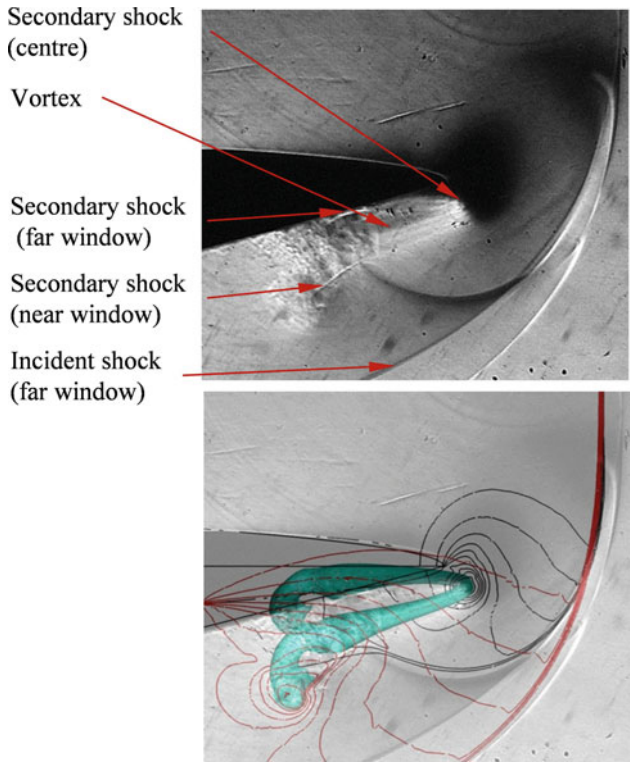

Fig. 5 Experimental and numerical results comparison, parabolic model, $M_s = 1.65$

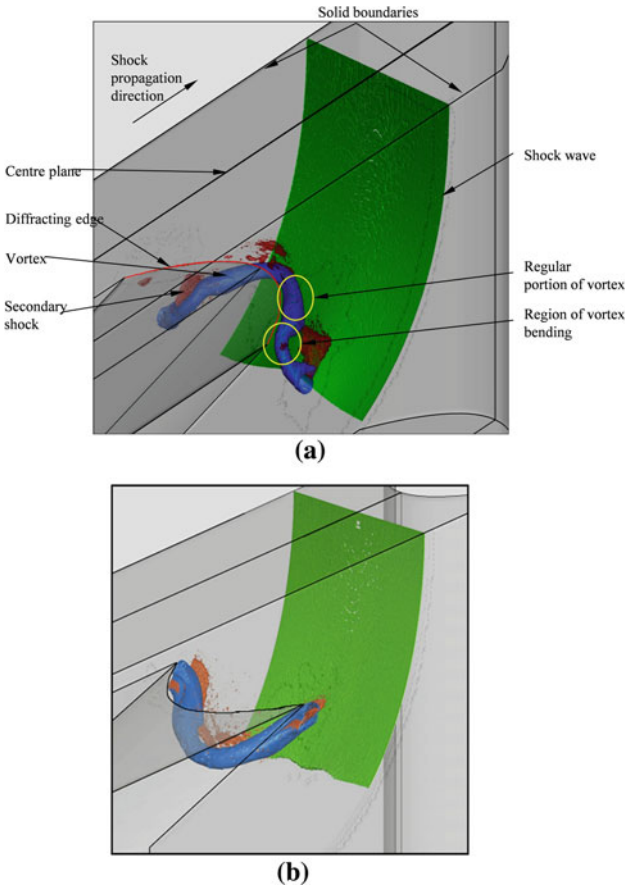

Fig. 6 Illustrations of typical flow field, **a** parabolic edge, **b** inverted parabolic edge ($M_s = 1.65$)

The images in Fig. 4 clearly show the distortion caused by the presence of the boundary on the vortex. Contraction of the vortex, as implied by (2), as the vortex core/axis is extended in the region near the boundaries as it is forced to bend so as to terminate at the boundary at a 90° angle, is also clearly illustrated. The presence of a secondary shock in the vortex is indicated in the red density contour lines at the near boundary. The slight distortion to the black contour lines to the right and left of the vortex indicates the presence of a secondary and tertiary shock, respectively, on the centre plane. Further investigation of the numerical results reveals these features to only be present in a small region near the solid boundary and centre plane. These features are indicated on the schlieren image in Fig. 5, and in Fig. 6 the extent to which they exist across the flow domain can be seen.

Validation of the numerical results against the experimentally obtained photographs was performed from visual comparisons. The correlation between the two sets of results is striking, and the complicated flow field and features were well captured in the numerical results for all models and time instants investigated. A comparison of the experimental and numerical images is given in Fig. 5, and the flow features discussed are labelled. A labelled illustration of a typical flow field for the parabolic model is given in Fig. 6a. Figure 6b gives a representation of the flow field for the inverted parabolic model for $M_s = 1.65$, for the incident shock wave at a similar distance away from the most upstream point of the diffracting edge as in Fig. 6a.

The results that have been dealt with here are for the $M_s = 1.65$ case. The solution is similar for $M_s = 1.42$, save for the lack of the secondary and tertiary shocks in the vortex. This was found to have negligible impact on the arrangement and profile that the vortex assumes. The flow field for the inverted parabolic diffracting edge revealed no further phenomena than that for the parabolic diffracting edge did. As a result, these results are not discussed in detail.

5.2 Description of flow field for 'V' models

The flow fields resulting from shock wave diffraction over the straight, 'V', edges are generally consistent with those mentioned above for the parabolic edges. The discontinuity in the diffracting edge (at the tip of the 'V') allowed for the meeting of two vortices with axes at an angle to one another to be investigated. The angle between the edge and the solid boundary was larger for the 'V' edges, 45°, whereas it was 25° for the parabolic edged model discussed previously. A set of schlieren images for $M_s = 1.65$ is given in Fig. 7.

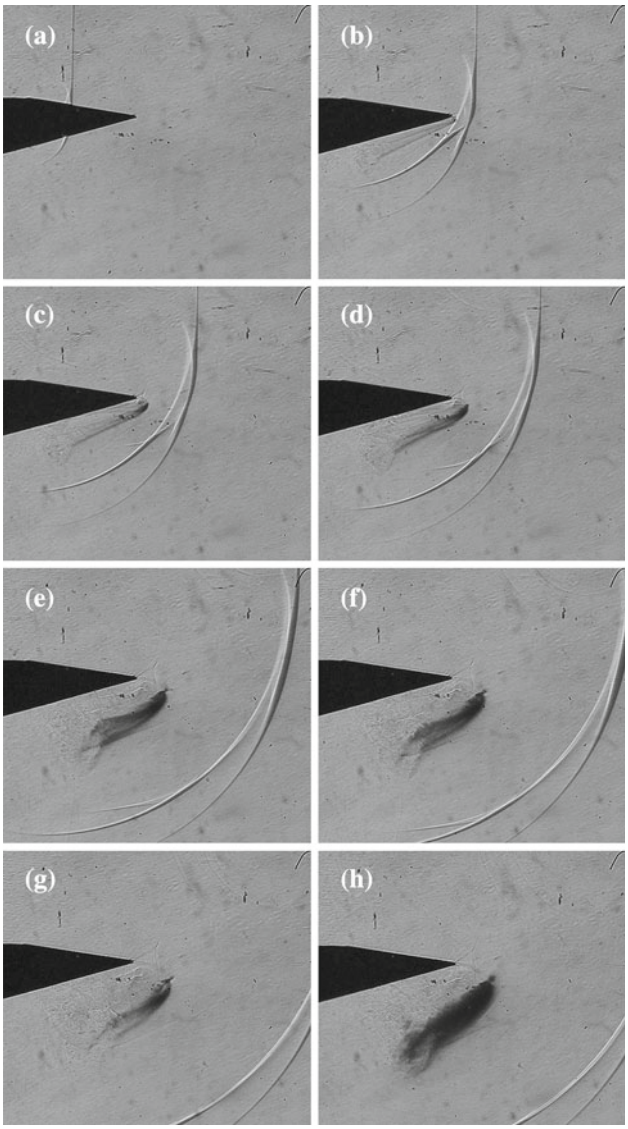

Fig. 7 Flow development, 'V' model, schlieren images taken at optical roll of 10°. $\Delta t = 25\,\mu s$ between images, $M_s = 1.65$

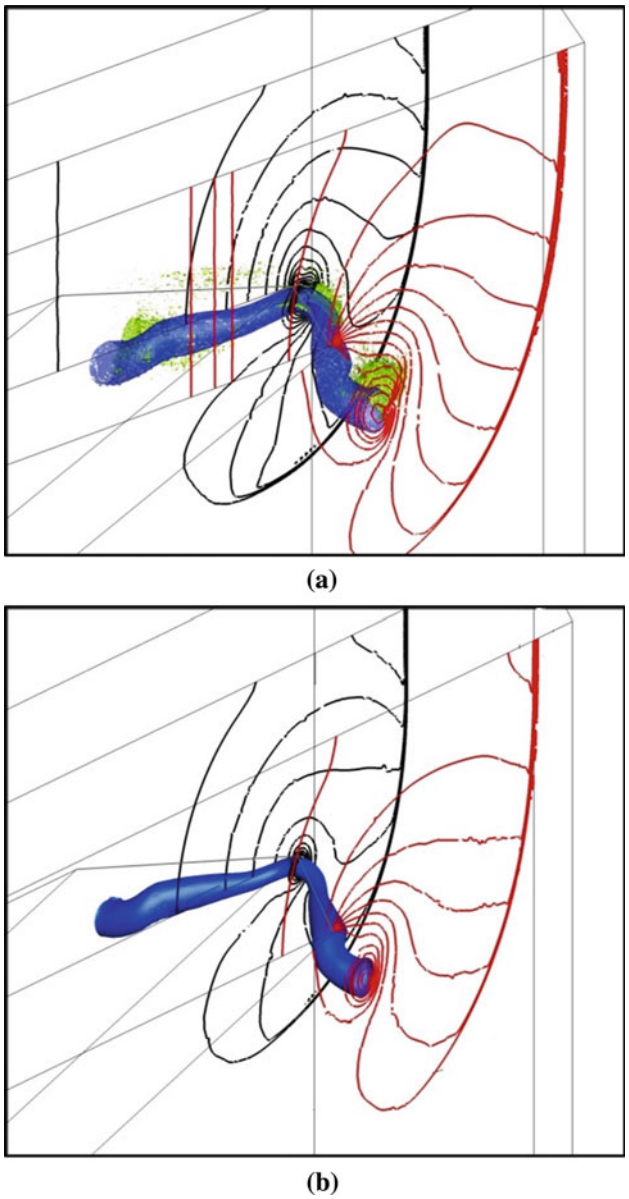

Fig. 8 'V' model, comparison of $M_s = 1.65$ and $M_s = 1.42$ flow fields. Vortex shown in *blue*, density contours plotted (*black* centre plane, *red* boundary), secondary and tertiary shocks in *green*. **a** $M_s = 1.65$, **b** $M_s = 1.42$

The images in Fig. 7 show that the vortex assumes an almost conical envelope away from the distortion caused by the presence of the windows. This is disrupted once the incident shock has fully diffracted over the edge, and the vortices on either side of the 'V' have met. From Fig. 7c onwards the distortion at the tip of the 'V', and that caused at the wall for that matter, propagates along the vortex axis, which appears curved along its entire length from Fig. 7e onwards. The behaviour of the vortex is discussed further in Sect. 6.

As with the previous case, numerical simulations have captured the flow features very well. Again, there is very little difference between the $M_s = 1.65$ and $M_s = 1.42$ cases. The only apparent difference is the presence of secondary and tertiary shocks in the vortex for $M_s = 1.65$. These have little effect on the shape and structure of the vortex, however. This can be seen in Fig. 8, where plots of the numerical results are given for both incident shock Mach numbers, with the incident shock in roughly the same position.

6 Vortex behaviour

All data pertaining to the spiral vortex is obtained from the numerical simulations. Top views of the evolution of the parabolic edge solution for $M_s = 1.65$ with time are given in Fig. 9. The incident shock wave is represented by the

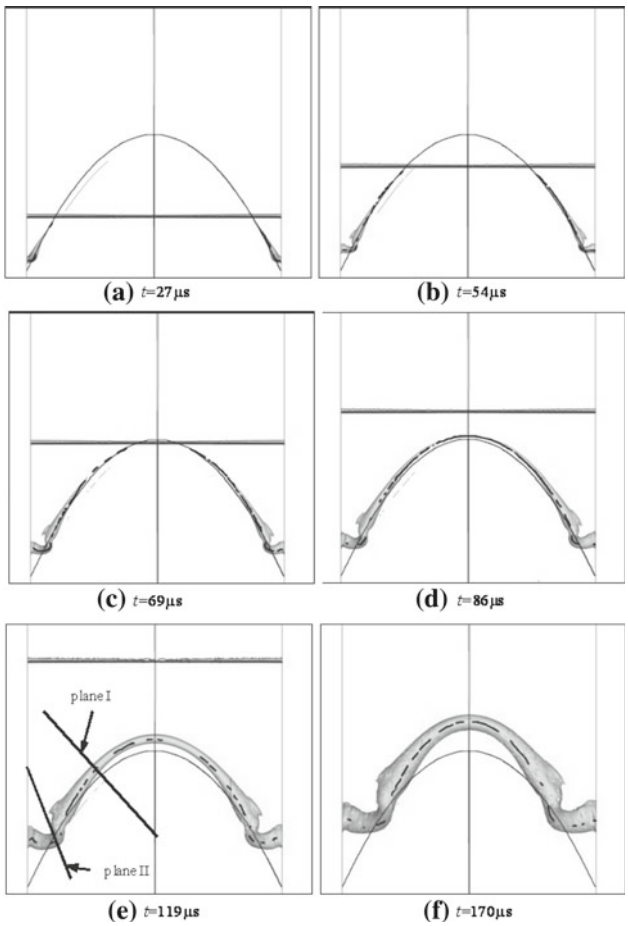

Fig. 9 Top view of vortex development, parabolic edge, $M_s = 1.65$, vortex core shown as *broken black line*

horizontal line, and the vortex cores, as extracted by Tecplot 360, are shown as a broken black line. The core extraction algorithm in Tecplot has some limitations, and as a result, the cores are not represented as a continuous line in the images that follow. The time instant $t = 0$ corresponds to the instant that the incident shock wave reaches the outer extremes of the diffracting edge, and begins to diffract.

The vortex has assumed a complicated geometry near the boundary, with the core bending so as to meet the boundary at a 90° angle. In the region between the distortions caused by solid boundaries on the left and right of the domain, the vortex assumes a near conical profile, although obviously its axis bends so as to conform to the diffracting edge profile. The vortex evolution appears almost self-similar in this region, as one would expect, based on the fact that the two-dimensional diffraction case and vortex produced are self-similar with time [4,5].

The structure of the vortex and the effects that bending has on it are demonstrated by data presented on two slices. These are taken perpendicular to the vortex axis from the top view taken through the vortex. The first (plane I) is taken through the region away from the distortion caused by the walls, and the second (plane II) through a region of bending. These planes are indicated in Fig. 9e. The data are taken on a horizontal line passing through the vortex core on each plane, the data are transformed such that the axial velocity component is in the vortex core direction at the cut (perpendicular to the plane). This data are presented in Fig. 10. Vorticity flood plots, showing the structure of the slipstream, are given on each of the two planes, at two time instants. The horizontal white line on these plots corresponds to the line on which the data are taken, and passes through the vortex core. The tangential, radial (positive to the right with reference to the images in the figures), axial velocity (positive out of the plane of the images in the direction of the vortex core, towards the nearest solid boundary), and normalised pressure plots are given. Note that the magnitude of the tangential velocity is given in the plots, with the flow in an anti-clockwise sense with reference to the images in the relevant figures. Data for the two time instants shown in the vorticity flood images is plotted. The vortex core is at zero on the x-axis in the plots. Note that the vortex core is not necessarily stationary. A small tangential and radial velocity is indicated at the vortex core in the plots that follow. It was decided to not subtract the vortex core velocity in presenting the data. This would misrepresent data from other parts of the flow field.

Considering the tangential velocity data on plane I, the first peak on the left is the outer spiral of the slipstream. The second peak is the beginning of the region of continuous vorticity magnitude that lies inside the slipstream spiral. The trough between the two peaks represents the region between the slipstream spirals. The apex of the trough thereafter is the vortex core. The final peak is the rightmost portion of the slipstream. The tangential velocity profile approximates that of a Rankine vortex, i.e. the tangential velocity is proportional to distance away from the core, near the core of the vortex. However, the slipstream disturbs this slightly by introducing variations into the tangential velocity. The bending of the vortex causes a greater gap between the outer spiral and core region of the slipstream, as can be seen by comparing the vorticity plots and the tangential velocity plots.

There is quite clearly a similarity between the data sets for the two time instants on plane I. This would imply a degree of self similarity in the evolution of the vortex with time in that region. There are obviously some slight discrepancies between the two data sets, caused by the non-uniform flow over the diffracting edge and the fact that this is a highly complicated three-dimensional flow field.

With regard to the data on plane I, the plots of radial velocity indicate a radial flow away from the core of the vortex. For $t = 86$ μs this is more pronounced than at the later time instant $t = 170$ μs. Note that the vortex core is not stationary, but move at approximately 30 m/s for both time instants to the left with reference to Fig. 10a and b.

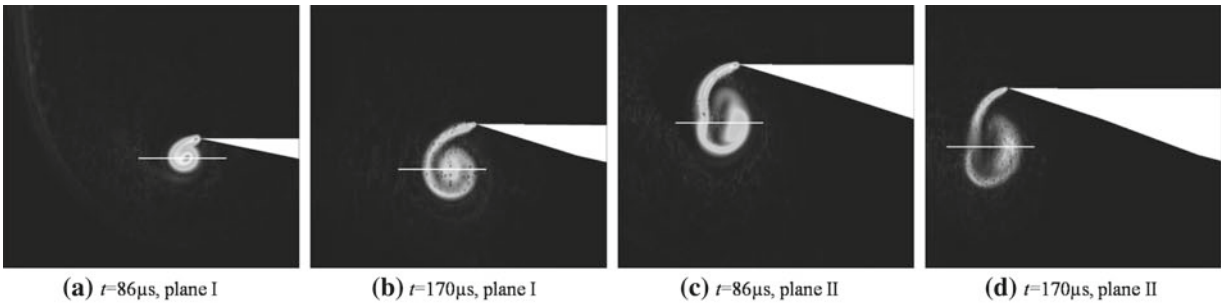

(a) t=86μs, plane I **(b)** t=170μs, plane I **(c)** t=86μs, plane II **(d)** t=170μs, plane II

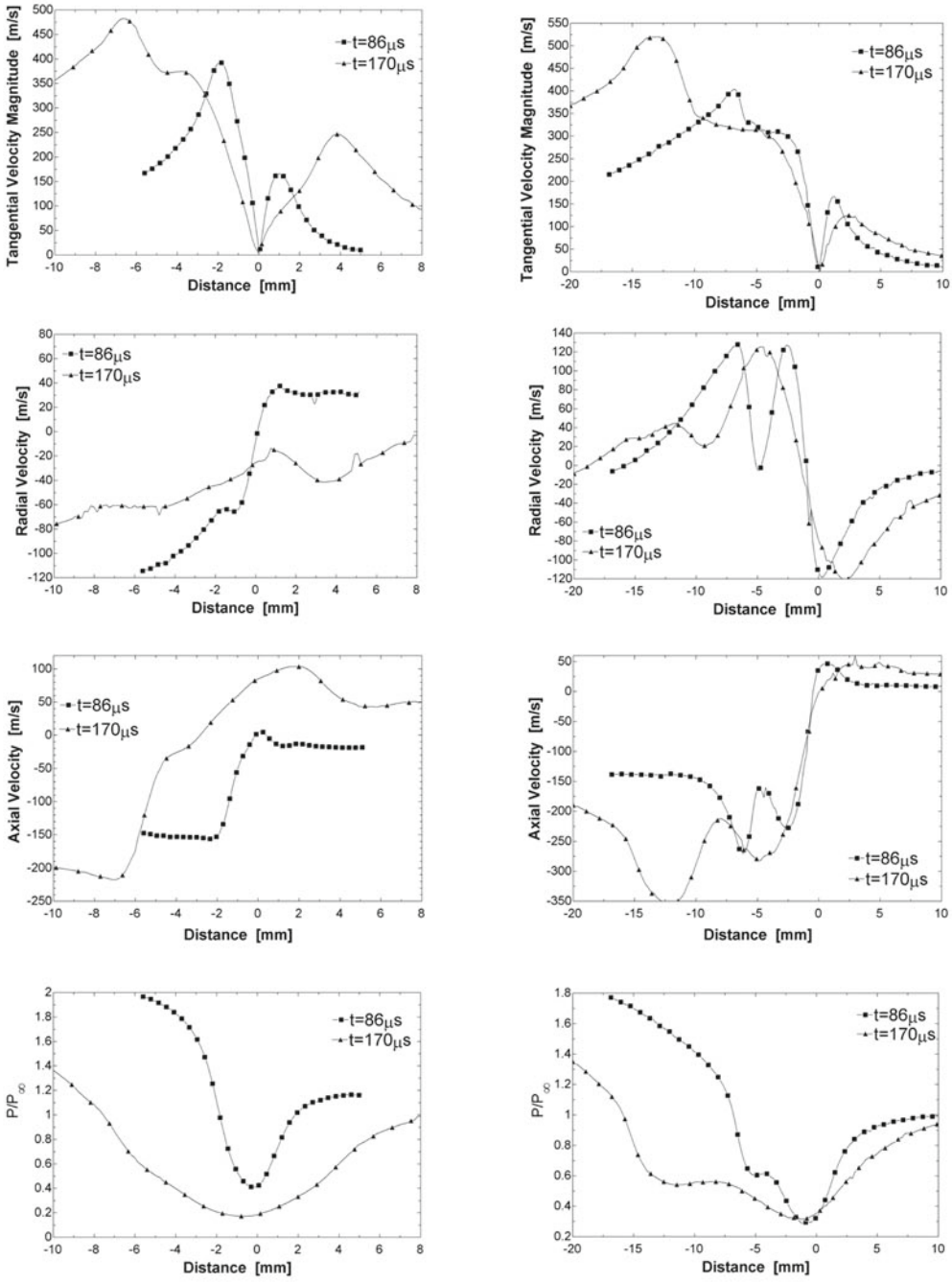

(e) Vortex property plots, plane I **(f)** Vortex property plots, plane II

Fig. 10 Vorticity plots and vortex property plots, parabolic edge, $M_s = 1.65$

The plots of axial velocity show significant differences on either side of the vortex core. For the plane I data, at $t = 86$ μs the velocity is approximately −150 m/s to the left of the core, and −20 m/s to the right of the core. At this location and time instant, the axial velocity at the core is approximately zero. At the later time instant $t = 170$ μs, the trend in the curve is similar. However, the velocity is now negative to the left of the core and positive to the right of the core.

The plane II data show that the bending of the vortex has had significant implications to the radial velocity distribution. On comparing the radial and axial velocities, and the pressure with that obtained previously, we see that a further trough now exists in the data due to the greater gap between the outer spiral and core region of the slipstream.

Plots of pressure, normalised by the reference pressure in front of the incident shock, are also given. The bending of the vortex distorts this plot slightly. A value of around 0.3 is typical at the core of the vortex. The pressure trends correlate quite closely with those published in the literature [1] for two dimensional vortices in the region away from the bend.

Figure 11 gives top views of the development of the vortex with time for the 'V' diffracting edge. Again, we see that the core has bent so as to meet the boundary at a 90° angle. There is a straight portion of the core, in the region away from the distortion caused by the presence of the solid boundary, before the vortices from either side of the 'V' have met. As the two vortices from either side of the 'V' meet each other, their cores bend so as to join and form a continuous curve.

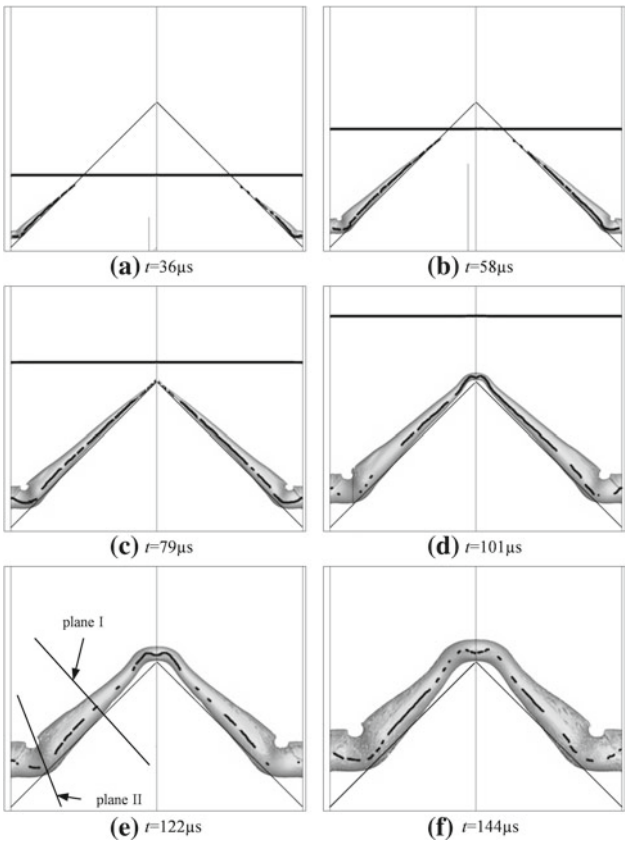

Fig. 11 Top view of vortex development, 'V' edge, $M_s = 1.65$, vortex core shown as *broken black line*

Data is plotted for two slices, shown in Fig. 11e, taken through the vortex, in a similar manner to the results given above. Plane I corresponds to the portion of the vortex where the core is straight, and undisturbed by distortions at the wall or centre of the flow domain. Plane II is taken through the vortex as it bends in the region near the solid boundary. Again, the data represented by the plots are taken on a horizontal line through the vortex core on each of the two planes.

Again, in the data taken on plane I, there is a similarity between the data taken at the two time instants. The velocity plots indicate a fair degree of self-similar vortex development in the regions away from the distortions to the vortex.

The tangential velocity plots show a fairly similar trend for a comparison of the data between the two planes. Similar observations to those made for the parabolic model above apply here. The radial velocity plots are fairly similar in nature, and there appears to be a slight correlation between the trends in the data sets taken on each plane. The plots of axial velocity show that there is significant and complicated axial flow within the vortex. As was highlighted previously, the velocity is lower to the left of the core than it is at the right of the core. The axial velocity is typically a maximum at the vortex core. The normalised pressure plots are similar to those for the parabolic model given above, and a value 0.3 is typical at the vortex core (Fig. 12).

7 Vorticity production

The rate of vorticity production in a two-dimensional shock diffraction case has been studied by numerous authors, most notably by Sun and Takayama [5]. Vorticity production data for all of the test models, each for incident shock Mach numbers of 1.42 and 1.65, were calculated.

A three-dimensional 'circulation' (Γ', normalised by RT_0, where R is the universal gas constant and T_0 the temperature in front of the incident shock) is evaluated by integrating the vorticity magnitude across the entire flow volume, this is plotted against time. Figure 13 gives a plot of the results.

The data for each shock Mach number tested tend to the same linear trend, after the initial curved portion of the plot, during which the shock wave is still in the process of diffracting over the edge. This would tend to indicate that the total rate of circulation production is independent of the diffracting edge profile, and that the fact that whether the edge is continuous or not (i.e. the parabolic edges vs. the 'V' edges) has little effect on the results.

There is a slight change apparent in the gradient of the linear portion of the curves in the region of $t = 150$ μs

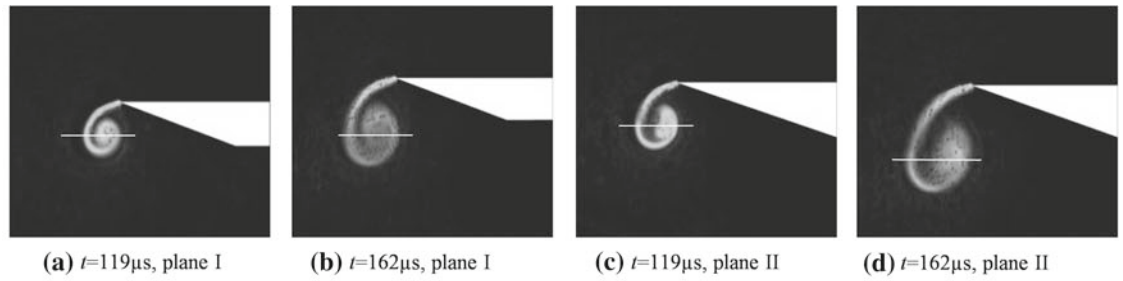

(a) t=119μs, plane I **(b)** t=162μs, plane I **(c)** t=119μs, plane II **(d)** t=162μs, plane II

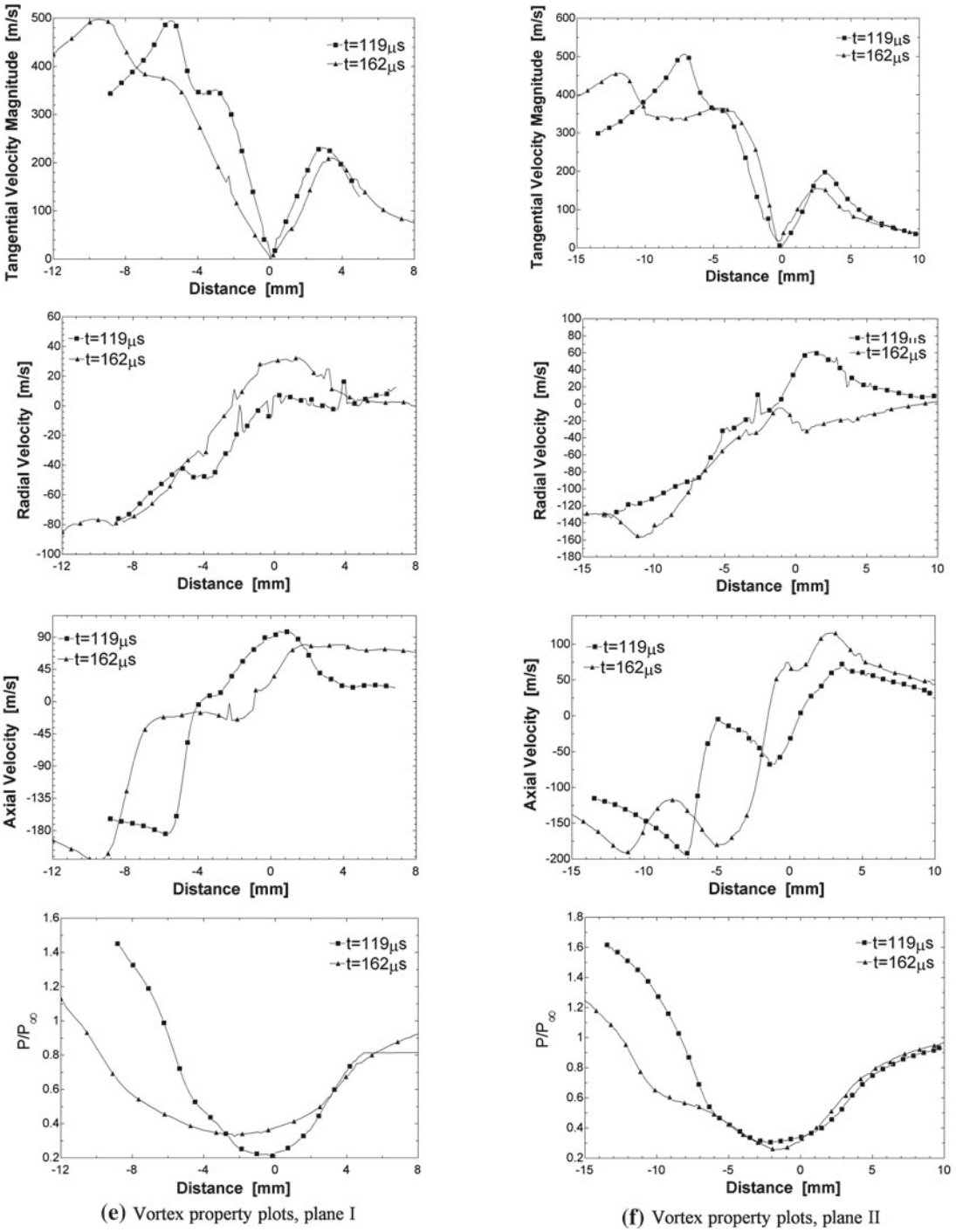

(e) Vortex property plots, plane I **(f)** Vortex property plots, plane II

Fig. 12 Vorticity plots and vortex property plots, 'V' edge, $M_s = 1.65$

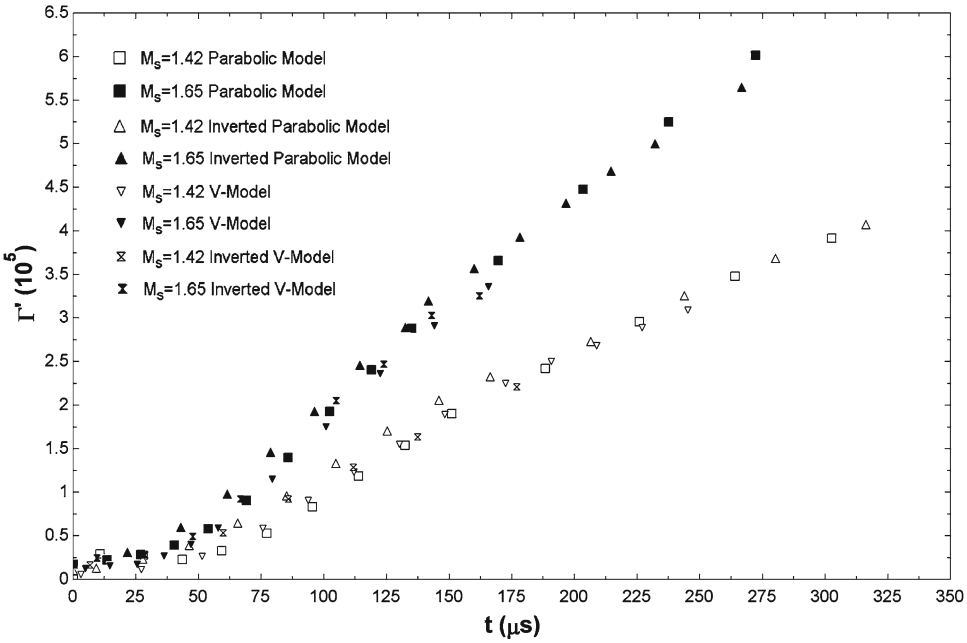

Fig. 13 Normalised circulation versus time

and $t = 135\,\mu s$ for the $M_s = 1.42$ and $M_s = 1.65$ cases, respectively. This anomaly is caused by the reflection of the expansion wave off of the top wall of the flow domain. The expansion wave first starts to reflect off of the top wall at approximately $t = 142\,\mu s$ for $M_s = 1.42$, and at approximately $t = 135\,\mu s$ for $M_s = 1.65$. This process appears to induce a slight downward curve in the data. As the reflected wave processes more of the flow volume, so the gradient of the curve appears to reduce further.

8 Conclusions

The numerical solutions captured the flow features very well, and good correlation between them and the experimental schlieren images was obtained. The spiral vortex was found to behave and bend in accordance with theoretical relations and laws given in the literature.

The vortex core bends so as to meet the solid boundaries at a 90° angle. The meeting of two vortices generated by a 'V' shaped diffracting edge was investigated, and the vortex cores were found to bend so as to form a continuous curve where the two vortices meet. The process and vortex behaviour were consistent with the bending in the region of a solid boundary. The vortex development and behaviour was, in general, consistent across the different incident shock Mach numbers tested (Mach 1.42 and 1.65) and four models tested. As would be expected, based on the previous two-dimensional shock diffraction studies, secondary and tertiary shocks appeared in the vortex for an incident shock Mach number of 1.65. These were only apparent in a region near the centre plane of the flow domain (all models tested were symmetrical about the centre plane) and the regions near the solid boundaries. They did not extend across the entire flow domain.

Flow properties (tangential, radial, and axial velocities, and the pressure profile) at different locations along the length of the vortex were presented, so as to investigate the effect that bending has on the structure of the vortex. Data were plotted for a conical region of the vortex apparently unaffected by distortions to the vortex, and for the region where the vortex is distorted and bends in the region near the solid boundary. The results showed a fair indication of self-similar vortex development with time in the region away from the distortions. The plots were distorted in the region of bending, where it was found so that a larger velocity magnitude existed on the side of the vortex towards the centre of curvature of the bend. The vortex was found to contract in the region of the bend, as if the core had been stretched.

The vorticity production was calculated for all the test models. The rate of vorticity production tended to a constant value once the incident shock wave had fully diffracted over the edge. The shape of the diffracting edge appeared to have no discernible impact on the results.

The meshes used in the three-dimensional simulations presented here were coarser than those used in the solution of typical two-dimensional diffraction cases published in the literature. Nevertheless, the results of the simulations presented here appear to have captured the flow field sufficiently well, as is evidenced by the good correlation obtained between the numerical and experimental work.

References

1. Bershader, B.W.: Compressible vortices. In: Green, S.I. (ed.) Fluid Vortices, pp. 291–315. Kluwer Academic, Dordrecht (1995)
2. Howard, L.N., Matthews, J.: On the vortices produced in shock diffraction. J. Appl. Phys. **27**, 223–231 (1956)
3. Saffman, P.G.: Vortex Dynamics. Cambridge University Press, London (1997)
4. Skews, B.W.: The perturbed region behind a diffracting shock wave. J. Fluid Mech. **29**, 705–719 (1967)
5. Sun, M., Takayama, K.: Vorticity production in shock diffraction. J. Fluid Mech. **478**, 237–256 (2003)
6. Tseng, T.I., Yang, R.J.: Numerical simulation of vorticity production in shock diffraction. AIAA J. **45**, 1040–1047 (2006)